



OPEN

Joint diffusional kurtosis magnetic resonance imaging analysis of white matter and the thalamus to identify subcortical ischemic vascular disease

Min-Chien Tu^{1,2}, Sheng-Min Huang³, Yen-Hsuan Hsu^{4,5}, Jir-Jei Yang⁶, Chien-Yuan Lin⁷ & Li-Wei Kuo^{3,8}✉

Identifying subcortical ischemic vascular disease (SIVD) in older adults is important but challenging. Growing evidence suggests that diffusional kurtosis imaging (DKI) can detect SIVD-relevant microstructural pathology, and a systematic assessment of the discriminant power of DKI metrics in various brain tissue microstructures is urgently needed. Therefore, the current study aimed to explore the value of DKI and diffusion tensor imaging (DTI) metrics in detecting early-stage SIVD by combining multiple diffusion metrics, analysis strategies, and clinical-radiological constraints. This prospective study compared DKI with diffusivity and macroscopic imaging evaluations across the aging spectrum including SIVD, Alzheimer's disease (AD), and cognitively normal (NC) groups. Using a white matter atlas and segregated thalamus analysis with considerations of the pre-identified macroscopic pathology, the most effective diffusion metrics were selected and then examined using multiple clinical-radiological constraints in a two-group or three-group paradigm. A total of 122 participants (mean age, 74.6 ± 7.38 years, 72 women) including 42 with SIVD, 50 with AD, and 30 NC were evaluated. Fractional anisotropy, mean kurtosis, and radial kurtosis were critical metrics in detecting early-stage SIVD. The optimal selection of diffusion metrics showed 84.4–100% correct classification of the results in a three-group paradigm, with an area under the curve of .909–.987 in a two-group paradigm related to SIVD detection (all $P < .001$). We therefore concluded that greatly resilient to the effect of pre-identified macroscopic pathology, the combination of DKI/DTI metrics showed preferable performance in identifying early-stage SIVD among adults across the aging spectrum.

Subcortical ischemic vascular disease (SIVD) is a common subtype of vascular cognitive impairment (VCI) in which cerebral vascular pathologies are spatially and pathologically stratified¹. Identifying SIVD in older adults is important but challenging². While white matter hyperintensities (WMHs) and lacunes within subcortical regions are pathognomonic in SIVD¹, these imaging features are also observed in patients with Alzheimer's disease (AD)³ and cognitively normal (NC) older adults⁴. To improve the detectability, exploring the value of advanced neuroimaging techniques is needed from both therapeutic and prognostic perspectives. Current diagnostic guidelines for dementia mostly describe neuroimaging features for individual dementia subtypes separately. Therefore, an optimized tool to assist in decision-making is needed, as clinicians often consider a list of differential diagnoses simultaneously in real-world practice. Among neuroimaging techniques, structural MRI has been shown to potentially be able to identify the presence of VCI among patients with dementia, and especially among those with AD^{5–7}. Compared to VCI, the early detection of SIVD is even more challenging, as the macroscopic

¹Department of Neurology, Taichung Tzu Chi Hospital, Buddhist Tzu Chi Medical Foundation, Taichung, Taiwan. ²Department of Neurology, School of Medicine, Tzu Chi University, Hualien, Taiwan. ³Institute of Biomedical Engineering and Nanomedicine, National Health Research Institutes, Miaoli, Taiwan. ⁴Department of Psychology, National Chung Cheng University, Chiayi, Taiwan. ⁵Center for Innovative Research on Aging Society (CIRAS), National Chung Cheng University, Chiayi, Taiwan. ⁶Department of Radiology, Taichung Tzu Chi Hospital, Buddhist Tzu Chi Medical Foundation, Taichung, Taiwan. ⁷GE Healthcare, Taipei, Taiwan. ⁸Institute of Medical Device and Imaging, National Taiwan University College of Medicine, Taipei, Taiwan. ✉email: lwkuo@nhri.edu.tw

plethora of WMHs and/or lacunes generally evolve later. Recently, diffusional kurtosis imaging (DKI) has been used to quantify microstructural changes, and it has been shown to improve the diagnostic accuracy of early-stage SIVD^{8–10}. To date, most DKI studies have focused on comparing cerebral microstructural changes among SIVD subgroups⁹ or with controls¹⁰, but few have compared SIVD with other dementia subtypes⁸. Moreover, it remains unclear which DKI metrics have the best performance in detecting SIVD amongst the aging spectrum. Importantly, the statistical power for differential diagnostics that is pivotal for clinical drug trials should be optimized by characterizing the underlying neurobiological heterogeneity¹¹. Given that the efficacy of DKI metrics can vary according to the targeted brain regions, macroscopic pathology, and clinical constraints, this study aimed to (i) investigate the diagnostic ability of DKI through two kinds of analytic strategies, (ii) validate the results either by considering multiple clinical constraints indicative of the very early stage of SIVD, or the effect driven by macroscopic pathology, and (iii) determine the optimal diffusion metrics to detect SIVD with a two-group or three-group paradigm.

Results

Demographics

Table 1 shows the basic information of the participants. There were group effects in demographics including age, education, and symptom duration (all $P < 0.001$), but not gender ($P = 0.224$). Other significant post-hoc differences were noted in WMHs (i.e., Scheltens scale and WMH volume; both $P < 0.001$; SIVD > AD > NC), the number of lacunes and Hachinski Ischemic Score (both $P < 0.001$; SIVD > NC and SIVD > AD), and global cognition (i.e., Mini-Mental State Examination (MMSE) and Cognitive Abilities Screening Instrument (CASI); both $P < 0.001$; SIVD < NC and AD < NC).

Diffusion metrics in the thalamus and white matter (WM)

Table 2 shows comparisons of diffusion metrics in the thalamus and WM after controlling for potential covariates including age, education, symptom duration, WMH volumes, and number of lacunes. Significant post-hoc results included: (i) in the thalamus, the SIVD group showed significantly lower fractional anisotropy (FA) and axial kurtosis (K_{axial}) than the AD group ($P = 0.011–0.041$), and significantly lower mean kurtosis (MK) and radial kurtosis (K_{radial}) than the NC group ($P = 0.043–0.044$); the AD group showed significantly higher mean diffusivity (MD), axial diffusivity (D_{axial}), and radial diffusivity (D_{radial}) than the NC group ($P = 0.003–0.019$), and (ii) in WM, the SIVD group showed significantly lower bilateral MK and K_{radial} ($P = 0.004–0.019$) than the NC group.

Diffusion metrics quantified in the white matter atlas (WMA) and segregated thalamus analysis (THA)

Table 3 shows the correct classification through discriminant analysis among the participants across the aging spectrum by diffusion metrics and macroscopic imaging evaluation in WMA and THA. At first glance, THA generally had a lower correct classification rate than WMA, but the trend among the performance of various diffusional kurtosis metrics was similar to that in WMA. Compared to correct classification by Scheltens scale (72.1%) and segregated WMH volume (63.9%), the use of mean kurtosis metrics in overall WMA achieved the highest correct classification rate (77.9%). Generally, FA showed higher correct classification rates than kurtosis fractional anisotropy (KFA) in all constraints except CDR. MK showed incrementally higher classification rates over MD in all cases (overall and three constraints) for both WMA and THA analyses. For both diffusivity and kurtosis, the mean and radial metrics generally showed higher correct classification rates than the axial metrics. Since KFA, D_{axial} , and K_{axial} showed relatively low correct classification rates, they were excluded from

	SIVD	AD	NC	F/χ^2 [§]	P
	(N = 42)	(N = 50)	(N = 30)		
Age (year)	73.5 ± 8.71	77.9 ± 5.05	70.5 ± 6.25	11.969 ^{ac}	<.001
Education (year)	5.5 ± 4.47	4.9 ± 4.62	9.4 ± 4.14	10.101 ^{bc}	<.001
Symptom duration (year)	1.5 ± 1.56	2.5 ± 2.22	0 ± 0.00	15.996 ^{abc}	<.001
Scheltens scale	24.7 ± 7.52	12.0 ± 6.59	7.3 ± 6.68	63.791 ^{abc}	<.001
White matter hyperintensities (ml)	38.8 ± 17.85	15.2 ± 14.64	6.3 ± 9.28	49.072 ^{abc}	<.001
Lacunes (number)	20.4 ± 13.75	8.6 ± 8.94	7.7 ± 8.48	17.616 ^{ab}	<.001
Hachinski Ischemic Score	10.0 ± 2.46	1.8 ± 1.45	1.9 ± 1.39	268.502 ^{ab}	<.001
Cognitive Abilities Screening Instrument	63.3 ± 14.55	59.1 ± 18.25	89.9 ± 4.58	44.572 ^{bc}	<.001
Mini-Mental State Examination	19.9 ± 5.03	19.1 ± 5.40	28.5 ± 1.07	43.875 ^{bc}	<.001
Gender (male/female) (N)	19/23	16/34	15/15	2.991	.224
Clinical Dementia Rating stage 0.5/1/2 (N)	25/12/5	22/24/4	–	3.634	.162

Table 1. Demographic of the participants. Data is represented as mean ± SD unless otherwise indicated. SIVD = Subcortical ischemic vascular disease. AD = Alzheimer's disease. NC = normal cognition. [§]The Analysis of Variance (ANOVA) and Chi-square test are used wherever appropriate. Significant between-group differences are remarked as ^aSIVD vs. AD; ^bSIVD vs. NC; ^cAD vs. NC. Median of white matter hyperintensities (SIVD/AD/NC/overall) = (37.4/10.2/2.2/14.2) ml. Median of the lacune number (SIVD/AD/NC/overall) = (17/7/4/8).

Metrics	Average white matter atlas				Average thalamus			
	SIVD	AD	NC	ANCOVA	SIVD	AD	NC	ANCOVA
	(N=42)	(N=50)	(N=30)	P	(N=42)	(N=50)	(N=30)	P
MK	.88 ± .071	.99 ± .606	1.05 ± .083	.004b	.81 ± .063	.89 ± .074	.92 ± .048	.031b
K _{axial}	.44 ± .030	.45 ± .025	.46 ± .021	.112	.45 ± .044	.44 ± .043	.45 ± .023	.014a
K _{radial}	1.16 ± .123	1.33 ± .098	1.41 ± .127	.019b	.97 ± .087	1.0 ± .088	1.1 ± .068	.037b
KFA	.35 ± .063	.38 ± .046	.39 ± .034	.866	.28 ± .087	.32 ± .069	.32 ± .038	.796
MD	1.20 ± .110	1.10 ± .068	1.03 ± .069	.102	1.32 ± .256	1.18 ± .207	.98 ± .093	.010c
D _{axial}	1.60 ± .093	1.52 ± .066	1.46 ± .061	.117	1.65 ± .281	1.53 ± .233	1.29 ± .100	.003c
D _{radial}	1.00 ± .123	.90 ± .072	.82 ± .075	.123	1.15 ± .245	1.01 ± .198	.823 ± .092	.019c
FA	.31 ± .039	.35 ± .024	.37 ± .030	.182	.27 ± .035	.30 ± .035	.30 ± .024	.047a

Table 2. Diffusional kurtosis and diffusion tensor metrics from the average thalamus and the white matter measures by groups. Data is represented as mean ± SD unless otherwise indicated. Mean/axial/radial diffusivity is presented in units of $10^{-3}\text{mm}^2\text{s}^{-1}$. P value from the analysis of covariance (ANCOVA) with covariates including age, education, symptom duration, the volume of white matter hyperintensities, and the number of lacunes are reported. The Tukey post-hoc comparisons are remarked as a: SIVD vs. AD; b: SIVD vs. NC; c: AD vs. NC. FA = Fractional Anisotropy. KFA = Kurtosis Fractional Anisotropy. MD = Mean Diffusivity. D_{radial} = Radial Diffusivity. D_{axial} = Axial Diffusivity. MK = Mean Kurtosis. K_{radial} = Radial Kurtosis. K_{axial} = Axial Kurtosis. SIVD = Subcortical ischemic vascular disease. AD = Alzheimer's disease. NC = normal cognition. Significant values are in bolditalics.

Metrics	White matter atlas*				Segregated thalamus analysis [§]			
	Overall	CDR ≤ 0.5	WMH ≤ 15 ml	Lacune ≤ 8	Overall	CDR ≤ 0.5	WMH ≤ 15 ml	Lacune ≤ 8
Scheltens scale [†]	72.1	72.7	67.2	72.6	–	–	–	–
Segregated WMH volume*	63.9	75.3	85.2	72.6	–	–	–	–
MK	77.9	81.8	81.0	77.4	68.9	76.6	80.3	79.0
K _{axial}	68.9	76.6	73.8	72.6	56.6	64.9	59.0	56.5
K _{radial}	74.6	80.5	78.7	83.9	66.4	64.9	70.5	69.4
KFA	66.4	75.3	78.7	75.8	58.2	63.6	70.5	66.1
MD	76.2	80.5	80.3	77.4	63.1	68.8	75.4	71.0
D _{axial}	76.2	76.6	78.7	74.2	55.7	67.5	73.8	74.2
D _{radial}	71.3	77.9	88.5	79.0	65.6	76.6	73.8	74.2
FA	72.1	75.3	88.5	79.0	66.4	72.7	77.0	69.4

Table 3. Discriminant analysis by diffusional kurtosis metrics, diffusion tensor metrics, and macroscopic imaging evaluation. Data are reported by the value of correct classification (%). CDR = Clinical Dementia Rating. WMH = white matter hyperintensities. FA = fractional anisotropy. MD = mean diffusivity. MK = mean kurtosis. KFA = kurtosis fractional anisotropy. D_{axial} = axial diffusivity. D_{radial} = radial diffusivity. K_{axial} = axial kurtosis. K_{radial} = radial kurtosis. SIVD = Subcortical ischemic vascular disease. AD = Alzheimer's disease. NC = normal cognition. Macroscopic imaging evaluation included the Scheltens scale and segregated WMH volume. [†]A total of 12 subregions averaged from bi-hemispheric ratings are used. *A total of 16 tracts including the corpus callosum (genu and body parts), and the anterior limb of internal capsule, anterior corona radiata, superior corona radiata, external capsule, cingulum (cingulate gyrus part), and superior longitudinal fasciculus of bi-hemispheres are used. [§]A total of 14 sub-regions of the thalamus including the pulvinar, anterior, mediodorsal, ventral-lateral-dorsal, central, ventral-anterior, and ventral-lateral-ventral nuclei are used. Cases number (SIVD/AD/NC): Overall = 42/50/30; CDR ≤ 0.5 = 25/22/30; WMH Volume ≤ 15 ml = 3/32/26; Lacunes ≤ 8 = 8/34/20.

comparisons of discrimination analyses using multiple metrics. Given a generally better performance in the measure of saving area of WMHs than the current measure aimed at region free from WMH, the statistical differences are not benefited by the process of WMH regional exclusion (Supplementary Table S1).

Optimized selection of multiple diffusion metrics

Figure 1 compares the performance of single diffusion metric and multiple diffusion metrics in discriminating the three groups. The correction classification rates of utilizing single/double/triple metrics from both hemispheres were 73.5/83.2/87.7% in WMA (Fig. 3A), and 66.1/75.0/77.9% in THA (Fig. 3B). In analysis of two hemispheres separately, the use of triple metrics showed correct classification rates of 80.7 and 72.3% in WMA and THA, respectively (Fig. 3A, B). Of note, the triple-metric usage of MK, K_{radial}, and FA achieved the best discriminant

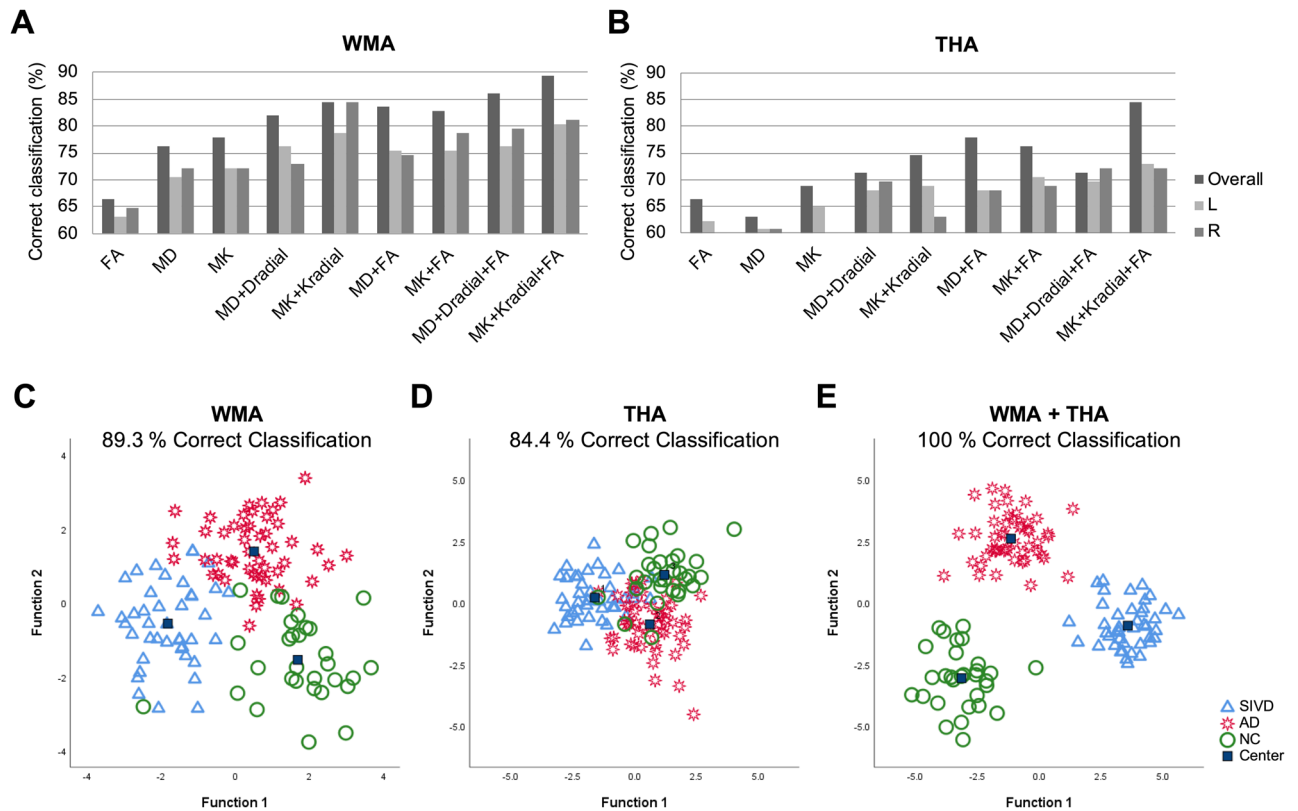


Figure 1. Discriminant analysis determined by kurtosis and diffusion metric selection. (A, B) Comparisons of variable metrics (e.g., MK, MD, and FA) by two measures (i.e., WMA and THA) shows that integration of triple metrics (MK + K_{radial} + FA) achieves the best discriminant analysis of aging spectrum including SIVD, AD, and NC (89.3% and 84.4% correct classification in the WMA and THA, respectively). In the WMA, the correct classification rate by single/double/triple metrics is 66.4–77.9/82.0–84.4/86.1–89.3%, with the averaged correct classification rate of 73.5/83.2/87.7%, respectively. In the THA, the correct classification rate by single/double/triple metrics is 63.1–68.9/71.3–77.9/71.3–84.4%, with the averaged correct classification rate of 66.1/75.0/77.9%, respectively. The correct classification rates of utilizing single/double/triple metrics were derived by entering the selected diffusion metrics (e.g. MK, MD, FA, ...etc.) from white matter atlas or thalamic atlas into to discriminant analysis. Data from different hemispheres were regarded as different inputs. Taking a triple-metric (MK + MD + FA) as an example, such triple-metric in bilateral WMA (total 16 regions) will give 48 values in each individual, and these 48 values are entered into discriminant analysis. The optimized kurtosis metrics (i.e., MK + K_{radial} + FA) is further examined by deciphering primary regions of interest by hemispheres, showing 80.7 and 72.3% average correct classification in the WMA and THA, respectively. (C–E) Discriminant analysis results from the optimized kurtosis metrics are plotted, showing that 89.3% correct classification in the WMA, 84.4% correct classification in the THA, and 100.0% correct classification in WMA + THA. R/L = Right/Left hemisphere. FA = fractional anisotropy; MD = mean diffusivity; MK = mean kurtosis; D_{radial} = radial diffusivity; K_{radial} = radial kurtosis. WMA = White matter atlas. THA = Segregated thalamus analysis. SIVD = Subcortical ischemic vascular disease. AD = Alzheimer’s disease. NC = normal cognition.

power across the aging spectrum (89.3/84.4% correct classification in WMA/THA) (Fig. 3C, D). Importantly, the use of both analysis strategies (i.e., WMA + THA) yielded a 100.0% correct classification rate (Fig. 3E).

ROC values from the optimal selection of triple diffusion metrics

Figure 2 shows the ROC curves for the sensitivity and specificity of optimal diffusion metrics to discriminate SIVD, AD and NC. To differentiate SIVD from AD, the highest AUC was for WMA (AUC = 0.964), followed by WMA + THA (AUC = 0.958) and THA (AUC = 0.909) (Fig. 4). To differentiate SIVD from NC (Fig. 4B), a similar trend was found (WMA > WMA + THA > THA; AUC = 0.987–0.965). Of note, all trials of the optimal DKI metrics aiming to detect SIVD yielded AUC values > 0.9. To differentiate AD from NC (Fig. 4C), WMA + THA achieved the best AUC of 0.953, followed by WMA (AUC = 0.937) and THA (AUC = 0.885) (all $P < 0.001$). Regarding individual regions, the tracts and nuclei showing the best statistical power were identified as (i) the left superior corona radiata and left ventral–lateral–ventral nuclei for SIVD vs. AD, (ii) the right anterior corona radiata and left ventral–lateral–ventral nuclei for SIVD vs. NC, and (iii) the right cingulum (cingulate gyrus part) and left central nuclei for AD vs. NC. Note that all belong to MK metrics (Supplementary Table S2).

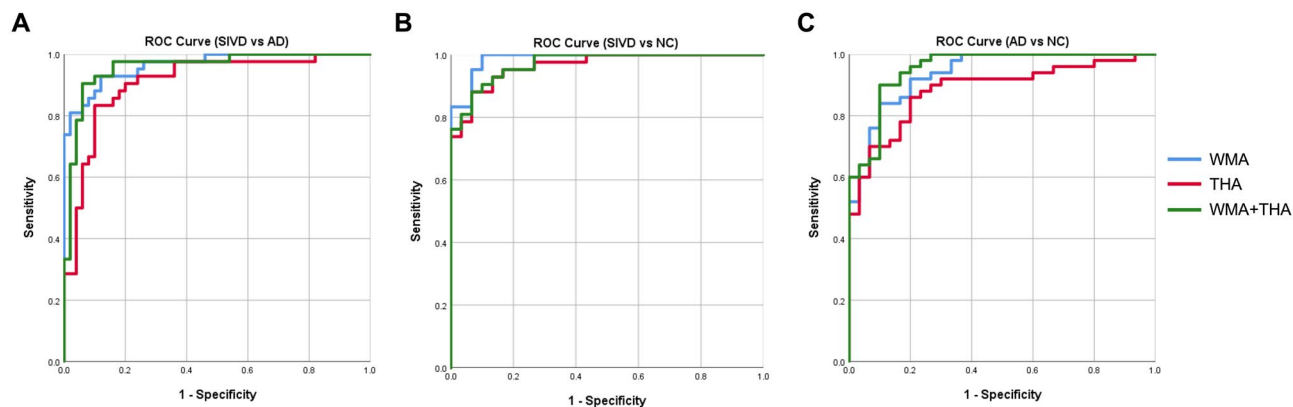


Figure 2. Optimized diffusional kurtosis metrics performance by receiver operating characteristic (ROC) curves. ROC curves were used to differentiating targeted diseased group. Ranked by AUC values, performance of optimized kurtosis metrics was displayed in (A) differentiating SIVD from AD by WMA [AUC = .964 (95% CI 0.932–0.997)], WMA + THA [AUC = .958 (95% CI 0.918–0.998)], and THA [AUC = .909 (95% CI 0.847–0.971)], (B) differentiating SIVD from NC by WMA [AUC = .987 (95% CI 0.969–1.000)], WMA + THA [AUC = .971 (95% CI 0.942–1.000)], and THA [AUC = .965 (95% CI 0.930–1.000)], and (C) differentiating AD from NC by WMA + THA [AUC = .953 (95% CI 0.908–0.997)], WMA [AUC = .937 (95% CI 0.886–0.988)], and THA [AUC = .885 (95% CI 0.881–0.958)]. WMA = White matter atlas. THA = Segregated thalamus analysis. SIVD = Subcortical ischemic vascular disease. AD = Alzheimer’s disease. NC = normal cognition. WMA = White Matter Atlas. T = Segregated thalamus. ROC = Receiver operating characteristic curves. AUC = Area under curve. CI = Confidence interval.

Correlates for global cognition

Table 4 shows the estimated effects of diffusion metrics on global cognition measured using the CASI. In the WMA, the right cingulum, right genu of the corpus callosum, and bilateral superior corona radiata were the best predictors ($P = < 0.001–0.035$). In THA, the nucleus including the left central, right ventral lateral-dorsal, right anterior, right mediodorsal, left pulvinar, and left ventral-anterior portions were significant ($P = < 0.001–0.023$).

Correlates for the Hachinski Ischemic Scale (HIS)

We also explored the associations between all diffusion metrics and the HIS. In the WMA, the bilateral anterior limbs of the internal capsule were the best predictors ($P = < 0.001–0.005$). In THA, the nucleus including

Metrics	White matter atlas				Segregated thalamus analysis			
	Regions	β	P	95% CI	Regions	β	P	95% CI
MK	CIN_R	.199	.024	(6.880,94.025)	C_L	.287	<.001	(36.722, 110.999)
K_{axial}	SCR_L	.222	.002	(24.535, 107.512)	VLD_R	.212	.002	(21.522, 96.746)
K_{radial}	SCR_R	-.265	.001	(-39.707, -9.655)	C_L	.311	<.001	(37.771, 100.090)
	CIN_R	.232	.004	(9.148, 47.426)				
KFA	SCR_R	-.195	.006	(-129.004, -21.908)	A_R	-.159	.023	(-77.130, -5.943)
MD	GCC_R	-.232	.002	(-26.495, -6.319)	Medio_R	-.296	<.001	(-21.756, -7.146)
D_{axial}	GCC_R	-.241	.001	(-29.636, -7.515)	P_L	-.375	<.001	(-46.005, -17.181)
D_{radial}	CIN_R	-.190	.034	(-46.284, -1.853)	Medio_R	-.287	<.001	(-22.153, -6.917)
	GCC_R	-.161	.035	(-20.748, -0.755)				
FA	SCR_R	-.279	<.001	(-181.874, -59.624)	VA_L	-.210	.004	(-159.212, -31.029)
	CIN_R	.252	.002	(32.160,142.450)				

Table 4. Estimated effect (β coefficients) of diffusional kurtosis and diffusion tensor metrics on global cognition ($N = 122$). Significant regions are reported by stepwise linear regression analysis, with independent variables including targeted imaging metrics showing significant correlation with the total scores of the Cognitive Abilities Screening Instrument. Metrics with a Variance inflation factor (VIF) ≥ 5 are removed. Estimated effect of all metrics is reported after controlling for age, education, symptom duration, the volume of white matter hyperintensities, and the number of lacunes. CIN = Cingulum. SCR = superior corona radiata. GCC = genu of the corpus callosum. A = anterior nuclei. C = central nuclei. P = pulvinar. VLD = ventral latero-dorsal. Medio = medio-dorsal. VA = ventral-anterior. R/L = Right/Left hemisphere. FA = fractional anisotropy. MD = mean diffusivity. MK = mean kurtosis. KFA = kurtosis fractional anisotropy. D_{axial} = axial diffusivity. D_{radial} = radial diffusivity. K_{axial} = axial kurtosis. K_{radial} = radial kurtosis. Mean/axial/radial diffusivity variables are entered in units of $10^{-3} \text{mm}^2 \text{s}^{-1}$.

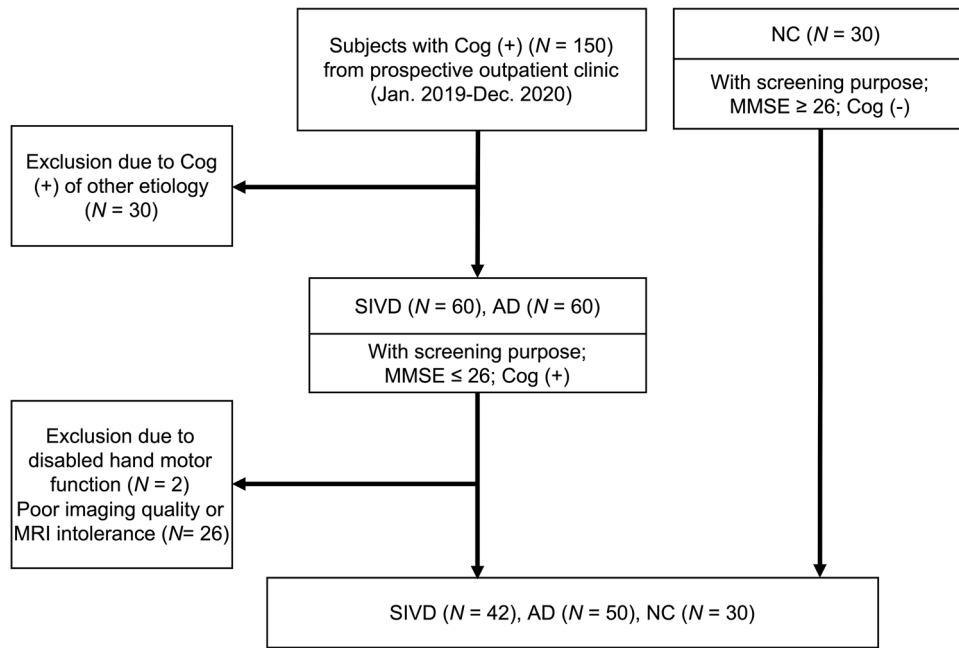


Figure 3. Flow Chart of Participants Selection. SIVD = Subcortical ischemic vascular disease; AD = Alzheimer’s disease; NC = normal cognition. Cog = Cognitive symptom. MMSE = Mini-Mental State Examination; MRI = magnetic resonance imaging.

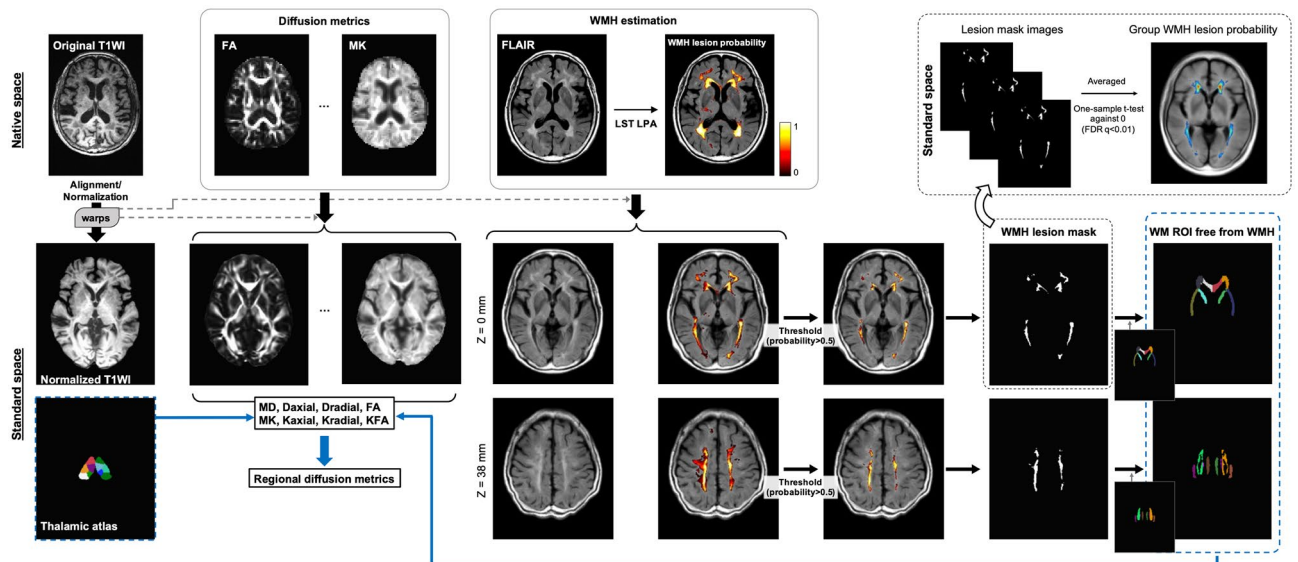


Figure 4. Illustration of the processing steps for MR images and the process for regional analysis. The diffusion metrics and the WMH probability maps were first estimated in native space, and consequently aligned on to standard MNI space according to the warp matrices from the co-registration process for T1WI (see Supplementary Materials for alignment details). The WMH maps were used to generated WMH lesion masks to calculate the WM ROIs free from WMH, and the WM ROIs free from WMH as well as the thalamic atlas were then utilized for the calculation of regional diffusion metrics. Group WMH lesion probability maps were also calculated as depicted in Supplementary Materials. T1WI = T1-weighted image. LST = Lesion Segmentation Tool. LPA = Lesion prediction algorithm. FDR = false discovery rate. WMHs = white matter hyperintensities. WM = white matter. FA = fractional anisotropy. MD = mean diffusivity. MK = mean kurtosis. KFA = kurtosis fractional anisotropy. Daxial = axial diffusivity. Dradial = radial diffusivity. Kaxial = axial kurtosis. Kradial = radial kurtosis.

the bilateral ventral latero-ventral, right ventral latero-dorsal, and right ventral-anterior were the significant ($P = 0.001–0.049$) (Supplementary Table S3).

Discussion

The current study shows the complementary value of using both diffusivity and kurtosis metrics. FA and DKI metrics in average THA could differentiate SIVD from AD and NC, and so could DKI metrics in average WMA. The selection of metrics was evaluated based on two analysis strategies (WMA and THA) and clinical-radiological constraints indicative of the very early stage of SIVD (e.g., WMH volume and number of lacunes). In the three-group discriminant analysis, we showed the power of DKI/DTI metrics in identifying SIVD. The optimal combination of metrics, i.e., MK, K_{radial} , and FA, yielded the highest correct classification rate. This combination was then validated using two-group comparisons via ROC analysis, which showed promising results overall. In addition, several WMA and THA hubs with significant effects in predicting global cognition anatomically overlapped with Papez and frontal-subcortical circuits, supporting the robustness of the diffusion metrics in exploring cognitive and neuronal substrates.

Our findings demonstrated that both DKI and DTI metrics provided better classification accuracy than Scheltens scale and segmented WMH volume. In average ROI analysis, MK performed incrementally better than MD across various clinical constraints. This corroborates the sensitivity inherited by the non-Gaussian premise assumption in DKI. It was also noticeable that the radial components of both kurtosis and diffusivity generally outperformed their axial components in terms of classification accuracy. Previous studies have shown that MK and K_{radial} exhibited a greater extent and degree of SIVD–AD differences than K_{axial} within the WM¹² and thalamus⁸. Another report has shown that radial metrics could possess higher sensitivity in detecting AD, mild cognitive impairment, and cognitively normal individuals¹³. As consistent with previous reports, the radial metrics could provide higher sensitivity in detecting the microstructural alterations especially in SIVD and AD. Hypothetically, liquefaction within the halo of lacunar/micro-infarcts and myelin pallor within WMHs¹⁴ could contribute to the geometrical variability of cerebral microstructures. We speculate that the attenuated discriminant power of K_{axial} may be due to diverse diffusing axis determination in the presence of neuronal and/or interstitial dispersion from vascular insults. This does not negate the importance of the axial components of kurtosis and diffusivity, and both K_{axial} and D_{axial} in our results could still differentiate SIVD or AD from NC. The importance of axial components was also suggested in a previously published AD cohort¹⁵. It is also worth mentioning that the classification rates of MK and MD improved remarkably with WMHs and lacunes as constraints in the thalamus rather than in WM. This effect of WMHs and lacunes could be associated with differences in regional vulnerability to vascular burden between WM and the thalamus, or the better inherited power of WMA than THA due to higher structural coherence within WM than the thalamus. Of note, independent evidence supports a viewpoint that the degree of DKI changes in response to ischemia differs according to the gray-white matter proportion of the affected regions¹⁶.

After controlling for demographics and macroscopic pathology including WMHs and lacunes, FA and DKI metrics enhanced SIVD–AD and SIVD–NC contrasts in the average THA, and DKI metrics solely enhanced SIVD–NC contrast in the average WMA. Aside from the reported role of FA in detecting vascular dementia⁶, our results further indicate that DKI is potentially resilient to the overall effect from WMHs and lacunes. It is also worth mentioning that DTI metrics enhanced AD–NC contrast in the average THA, demonstrating the complementary value of DKI and DTI metrics. KFA and FA had similar tendencies in most comparisons, but KFA showed a lower correct classification rate than FA. As the DKI metrics were derived from a WMA driven by FA, the possibility of pseudo-normalization of KFA values when the quantification process involves crossing fibers as documented issues in FA calculations should be considered¹⁷. The numeric accuracy of KFA may also have been overwhelmed since WM and microstructure coherence was already compromised by vascular burden, and hence it may be a less promising metric in terms of test–retest reliability¹⁰ and statistical power⁹.

In this study, we used a WMA *free* from WMHs while considering WMHs and lacunes as statistical covariates, which is a two-tier concept. First, measurements focusing on normal-appearing WM could provide information presumably corresponding to pathological alterations at the very early stage of SIVD. Second, the additional statistical considerations reduced the effect driven by vascular pathology, which had already been identified macroscopically and may have had an indirect effect due to Wallerian degeneration. Of note, our results bridge the published findings^{8,18} by highlighting that a joint analysis strategy is a favorable solution for constructing a dementia classifier across the aging spectrum. We consider that the joint analysis strategy integrating both gray and WM is an informative ensemble which can be used to stratify the subtype of dementia across the aging spectrum. This also mirrors the regional/tissue vulnerability inherently associated with individual dementia subtypes. As we only investigated two dementia subtypes and cognitively normal older adults, identifying dementia subtypes other than SIVD or AD falls beyond the scope of discussion.

Our results connect neuronal substrates associated with global cognition to some specific WM hubs, including the genu of the corpus callosum and cingulum of the right hemisphere, and the bilateral superior corona radiata. In addition, THA delineated a pervasive pattern scattered across multiple thalamic nuclei. The overall hubs identified in this study considerably overlapped with landmarks belonging to the Papez circuit or frontal-subcortical circuit¹⁹. As the interplay between these two circuits plays a critical role in harmonizing global cognition¹⁹, using diffusional kurtosis metrics could provide additional value in exploring neuronal substrates critical for cognition. In addition, the current metrics exhibit pervasive correlations with the HIS, and the significance remains in considering demographics and indices of cerebral small vessel disease. This corroborates that the diffusional kurtosis metrics can be regarded as potential biomarkers that mirror the composite vascular risk in the aging spectrum. The strength of this study is the integration of WMA and THA analysis strategies with several clinical-radiological constraints targeting the very early stage of SIVD. Diffusion metrics were derived and compared

with macroscopic pathology including WMHs and lacunes, and the results showed that combining DKI and DTI metrics could provide robust differential power and resilience to predefined vascular lesions. Moreover, the optimal combination of diffusion metrics showed robust performance in two- or three-group comparisons, suggesting its potential for clinical applications. There are also several limitations to the study. Not all dementia subtypes were included, and the prevalence of dementia subtypes varies across medical settings. Including more dementia subtypes in future studies may provide an opportunity to investigate the robustness and improve the optimal selection of diffusion metrics. In addition, the insignificant differences of diffusional kurtosis metrics between AD and NC within WM could be related to the excluding the effect of WMHs by both imaging processing and statistics. Since the effect of WMHs has been minimized, we believe that the diffusion metrics used in this study provide a reliable reference for future application in differential diagnostics.

In conclusion, the current study investigates the sensitivity and resilience of diffusion metrics for macroscopic vascular lesions that are pathognomonic to SIVD. The optimal combination of diffusion metrics included MK, K_{radial} , and FA, which could effectively differentiate SIVD from other groups across the aging spectrum in both WMA and THA strategies ($AUC > 0.9$). The joint analysis strategy showed the best performance. The additional and complementary values of the diffusion metrics were comprehensively explored as hubs for global cognition identified and anatomically overlapped with Papez and frontal-subcortical circuits.

Methods

Study design and participants

This prospective, observational, cross-sectional single-center study was approved by the Research Ethics Committee of Taichung Tzu Chi Hospital (#REC-107-28). Written informed consent was obtained from all participants. A total of 150 subjects with cognitive complaints from an outpatient dementia clinic were consecutively screened from January 2019 to December 2020 (Fig. 3). Those with clinical assessments showing cognitive complaints, brain CT showing no cortical encephalomalacia, and a MMSE score ≤ 26 were initially included; those with incomplete cognitive assessment and brain MRI scans were excluded. SIVD was diagnosed using the research criteria proposed by Erkinjuntti et al.¹; AD was diagnosed using the National Institute of Neurological and Communicative Disorders and Stroke and the Alzheimer's Disease and Related Disorders Association criteria²⁰; patients with mixed dementia were excluded if the Hachinski Ischemic Scale was 5–6²¹. As the published⁸, the inclusion and exclusion criteria were presented in Supplementary Table S4 Overall, 42 patients with SIVD and 50 with AD were recruited in this study. In addition, another 30 older adults who showed no cognitive symptoms and had an MMSE score ≥ 26 were recruited as the NC group. There is some overlap of these participants with a previously published article²², however the analysis approaches were different from the current study.

Clinical data collection

We recorded age, gender, education, cognitive symptom duration, and Hachinski Ischemic Score. WMHs were rated according to Scheltens scale (a total of 12 subregions within the supra-tentorial parts)²³ by a neurologist (M.C.T.) with 11 years of experience, and quantified using the Lesion Prediction Algorithm (LPA)²⁴. The LPA results, morphology of the thalamus, and number of lacunes were visually assessed by the same neurologist. Global cognitive scores including the MMSE, CASI, and Clinical Dementia Rating were rated by a team of certified clinical psychologists led by Y.H.H., who has 8 years of experience.

MRI protocols

The brain MR images were obtained at a 3 T MRI scanner (Discovery MR750, GE HealthCare, Milwaukee, WI) with an eight-channel phased-array head coil. The following protocols were acquired: three-dimensional T1-weighted imaging (3D-T1), T2 fluid-attenuated inversion recovery imaging (T2-FLAIR), and diffusional kurtosis imaging (DKI). For 3D-T1, a fast spoiled gradient echo with RF-spoiling (FSPGR) was performed with repetition time (TR) of 7.90 ms, echo time (TE) of 3.06 ms, inversion time (TI) of 450 ms, flip angle of 12°, matrix size (MTX) of 240 × 240 × 160, achieving an isotropic voxel size of 1 mm³. Parameters for T2-FLAIR were TR of 12,000 ms, TE of 120 ms, TI of 2200 ms, field-of-view (FOV) of 220 mm, MTX of 384 × 224, 21 slices with slice thickness (SL) of 5 mm. Spin-echo diffusion-weighted echo-planar imaging was used to obtain DKI datasets. A total of 30 diffusion gradient directions were obtained with two b -values (1000 and 2000 s/mm²) along each direction, and 5 un-weighted images (b_0 , $b = 0$ s/mm²) were acquired, resulting a total of 65 volumes for DKI dataset. Other scanning parameters were TR of 6000 ms, TE of 68 ms, FOV of 240 mm, MTX of 96 × 96, 60 slices with SL of 2.5 mm, resulting an isotropic spatial resolution of 2.5 mm³.

MRI analysis

Image processing

Figure 4 illustrates the processing steps for MRI data (S.M.H. and L.W.K., with 12 years and 22 years of experience, respectively). All image processing and registration steps were performed using AFNI software (<https://afni.nimh.nih.gov>)²⁵. All of the 3D-T1 images were aligned and normalized into standard MNI space, and all of the spatial warping transformation matrices were utilized for the alignment of the DKI-derived metrics^{26,27}. Initially, the 3D-T1 image were skull-stripped and roughly registered with the MNI T1 template via 12-parameter affine alignment. After initial alignment, tissue segmentation was performed on the roughly-aligned T1 image to identify white matter, gray matter, and cerebrospinal fluid (CSF). CSF voxels were set to zero to generate the CSF-free T1 image. The same masking process was performed on the MNI T1 template to generate the CSF-free MNI T1 template. After this process, a two-step non-linear warping process was employed for better co-registration outcome. First, the CSF-free 3D-T1 image was co-registered to the CSF-free MNI T1 template by using non-linear co-registration, and this output non-linear warping transformation was then applied on the

roughly-aligned 3D-T1 images to generate the first warped 3D-T1 image. The first warped 3D-T1 image was then non-linearly co-registered to the MNI T1 template again to form the final aligned 3D-T1 image. As the size of ventricle varies across subjects, the two-step procedure was carried out to achieve adequate image alignment results. All of the warp parameters and transformation matrices derived from the alignment process were used for the following alignment of diffusion weighted images (DWIs).

DKI reconstruction

The DKI data analyses were implemented using in-house MATLAB scripts (MathWorks, MA, USA). Before DKI reconstruction process, all the DWIs were denoised with local PCA method²⁸. DKI reconstruction was performed according to the estimation approach of DKI model proposed by Tabesh et al.²⁹. The DKI data was fit to the DKI model using the Levenberg–Marquardt algorithm with least-squared error estimations. The diffusivity and kurtosis metrics along all diffusion gradient directions were derived and averaged by using diffusion data with all b-values (i.e., 1000 and 2000 s/mm²). The quantitative metrics of DTI (MD; D_{axial} ; D_{radial} ; FA) and DKI (MK; K_{axial} ; K_{radial} ; KFA) were then calculated from the DKI model. The diffusion metrics were first estimated in each subject's native space, and then the DKI parametric maps were aligned to MNI space according to the transformations from the following alignment process on DWIs. First, the b0 images were aligned to each subject's own 3D-T1 images via 12-parameter affine alignment. Second, the T1-related transformation matrix and warp parameters described in previous section ('Image processing') were applied onto the T1-aligned b0 image to generate aligned b0 image in the MNI space. Finally, the DKI parametric maps were aligned to MNI space by applying the same transformations previously determined on b0 images. To reduce potential registration bias surrounding the edge of ventricular space and thalamus, a ventricle mask was generated from averaged b0 images of the SIVD group by AFNI software to avoid including unwanted ventricular voxels when calculating the regional DKI metrics.

WMH volume assessment

We performed automatic WMH segmentation by using the LPA^{24,30} as implemented in the lesion segmentation tool (LST 3.0.0, <https://www.applied-statistics.de/lst.html>) for SPM. This algorithm utilizes FLAIR images to estimate the lesion probability of white matter. The segmentation result of each subject was visually inspected by an experienced neurologist (M.C.T.). To calculate the total volume of WMH, we used LST's default settings of probability threshold of 0.5 (probability of a voxel being WMH) (Supplementary Figure S1).

Regional diffusion metric

In the WMA, a total of 16 tracts including the corpus callosum (genu and body parts), the anterior limb of the internal capsule, anterior corona radiata, superior corona radiata, external capsule, cingulum (cingulate gyrus part), and superior longitudinal fasciculus of bi-hemispheres were used based on the JHU DTI-based white-matter atlases available in FSL (<https://fsl.fmrib.ox.ac.uk/fsl/fslwiki/Atlases>). In the WMA, pixels with WMHs are excluded according to the LPA method described above, and hence the measurements focus on WM *free* from WMHs. In the THA, a total of 14 thalamic sub-regions including the pulvinar, anterior, mediodorsal, ventral–lateral–dorsal, central, ventral-anterior, and ventral–lateral–ventral nuclei were used based on a segregated thalamic atlas³¹.

Statistical analysis

Analysis of variance and the chi-square test were used to compare demographic data. Analysis of covariance with Tukey post hoc comparison was used to compare diffusion metrics by controlling for age, education, symptom duration, volume of WMHs, and number of lacunes. After exploring the performance of diffusion metrics using discriminant analysis with clinical and macroscopic imaging constraints, receiver operating characteristic (ROC) curves were further used to examine the ability of the selected diffusion metrics to detect SIVD. The key goal of serial discriminant analyses aimed at identifying which diffusional kurtosis metric(s) perform the best value of correct classification. The purpose of additional analyses for examining both hemispheres or single hemisphere was to present the effect related to number of variables fed into the discriminant analyses as well as intra-group variation, if any. The rationale to include clinical and macroscopic imaging constraints was to examine the current diffusional kurtosis metrics among those population with a relatively early dementia stage (i.e., CDR \leq 0.5) or limited cerebral vascular burden (i.e., WMH \leq 15 ml and lacune number \leq 8). To constrain composite diffusion metrics from multiple regions of interest, binary logistic regression was used to derive probability values of diffusion metrics in each ROC trial. Pearson correlation analysis was used to quantify relationships between diffusion metrics and cognitive parameters. Stepwise linear regression analysis was used to identify estimated effects of diffusion metrics on cognition. All statistical tests were performed using SPSS version 25 (IBM, Armonk, NY). A *P* value < 0.05 was considered statistically significant.

Ethics declarations

This study was performed in line with the principles of the Declaration of Helsinki. Approval was granted by the Research Ethics Committee of our Hospital (#REC-107-28).

Consent to participate

Informed consent was obtained from all individual participants included in the study.

Data availability statement

Data generated or analyzed during the study are available from the corresponding author on reasonable request.

Received: 12 September 2023; Accepted: 25 January 2024

Published online: 31 January 2024

References

- Erkinjuntti, T. *et al.* Research criteria for subcortical vascular dementia in clinical trials. *Adv. Dementia Res.*, 23–30 (2000).
- Tu, M.-C. *et al.* Effectiveness of diffusion tensor imaging in differentiating early-stage subcortical ischemic vascular disease, Alzheimer's disease and normal ageing. *PLoS ONE* **12**, e0175143 (2017).
- Attens, J. & Jellinger, K. A. The overlap between vascular disease and Alzheimer's disease-lessons from pathology. *BMC Med.* **12**, 1–12 (2014).
- Smith, E. E. *et al.* Early cerebral small vessel disease and brain volume, cognition, and gait. *Ann. Neurol.* **77**, 251–261 (2015).
- Koikkalainen, J. *et al.* Differential diagnosis of neurodegenerative diseases using structural MRI data. *NeuroImage: Clin.* **11**, 435–449 (2016).
- Zarei, M. *et al.* Regional white matter integrity differentiates between vascular dementia and Alzheimer disease. *Stroke* **40**, 773–779 (2009).
- Lambert, C. *et al.* Identifying preclinical vascular dementia in symptomatic small vessel disease using MRI. *NeuroImage: Clinical* **19**, 925–938 (2018).
- Tu, M. C. *et al.* Discriminating subcortical ischemic vascular disease and Alzheimer's disease by diffusion kurtosis imaging in segregated thalamic regions. *Hum. Brain Mapp.* **42**, 2018–2031 (2021).
- Liu, D. *et al.* Correlations between the microstructural changes of the medial temporal cortex and mild cognitive impairment in patients with cerebral small vascular disease (cSVD): A diffusion kurtosis imaging study. *Front. Neurol.* **10**, 1378 (2020).
- He, X., Dou, W. & Shi, H. The diagnostic value of the combined 3D pseudo-continuous arterial spin labeling and diffusion kurtosis imaging in patients with Binswanger's disease. *Front. Neurosci.* 1027 (2022).
- Lawrence, A. J. *et al.* Pattern and rate of cognitive decline in cerebral small vessel disease: A prospective study. *PLoS ONE* **10**, e0135523 (2015).
- Raja, R., Caprihan, A., Rosenberg, G. A., Rachakonda, S. & Calhoun, V. D. Discriminating VCID subgroups: A diffusion MRI multi-model fusion approach. *J. Neurosci. Methods* **335**, 108598 (2020).
- Chu, X. *et al.* Comparison of brain microstructure alterations on diffusion kurtosis imaging among Alzheimer's disease, mild cognitive impairment, and cognitively normal individuals. *Front. Aging Neurosci.* **14**, 919143 (2022).
- Erten-Lyons, D. *et al.* Neuropathologic basis of white matter hyperintensity accumulation with advanced age. *Neurology* **81**, 977–983 (2013).
- Nir, T. M. *et al.* Effectiveness of regional DTI measures in distinguishing Alzheimer's disease, MCI, and normal aging. *NeuroImage: Clin.* **3**, 180–195 (2013).
- Zhu, L.-H., Zhang, Z.-P., Wang, F.-N., Cheng, Q.-H. & Guo, G. Diffusion kurtosis imaging of microstructural changes in brain tissue affected by acute ischemic stroke in different locations. *Neural Regeneration Research* **14**, 272 (2019).
- Douaud, G. *et al.* DTI measures in crossing-fibre areas: Increased diffusion anisotropy reveals early white matter alteration in MCI and mild Alzheimer's disease. *Neuroimage* **55**, 880–890 (2011).
- Praet, J. *et al.* Diffusion kurtosis imaging allows the early detection and longitudinal follow-up of amyloid- β -induced pathology. *Alzheimer's Res. Ther.* **10**, 1–16 (2018).
- McNaughton, N. & Vann, S. D. Construction of complex memories via parallel distributed cortical-subcortical iterative integration. *Trends Neurosci.* (2022).
- McKhann, G. M. *et al.* The diagnosis of dementia due to Alzheimer's disease: Recommendations from the National Institute on Aging-Alzheimer's Association workgroups on diagnostic guidelines for Alzheimer's disease. *Alzheimer's Dementia* **7**, 263–269 (2011).
- Hachinski, V. C. *et al.* Cerebral blood flow in dementia. *Arch. Neurol.* **32**, 632–637 (1975).
- Tu, M.-C., Chung, H.-W., Hsu, Y.-H., Yang, J.-J. & Wu, W.-C. Stage-dependent cerebral blood flow and leukoaraiosis couplings in subcortical ischemic vascular disease and Alzheimer's disease. *J. Alzheimer's Dis.* 1–12 (2022).
- Scheltens, P. *et al.* A semiquantitative rating scale for the assessment of signal hyperintensities on magnetic resonance imaging. *J. Neurol. Sci.* **114**, 7–12 (1993).
- Schmidt, P. *Bayesian inference for structured additive regression models for large-scale problems with applications to medical imaging*. lmu (2017).
- Cox, R. W. AFNI: Software for analysis and visualization of functional magnetic resonance neuroimages. *Comput. Biomed. Res.* **29**, 162–173 (1996).
- Nowrangi, M. A. *et al.* Atlas-based diffusion tensor imaging correlates of executive function. *Journal of Alzheimer's Disease* **44**, 585–598 (2015).
- Baijot, J. *et al.* Radial diffusivity reflects general decline rather than specific cognitive deterioration in multiple sclerosis. *Scientific Reports* **12**, 21771 (2022).
- Manjón, J. V. *et al.* Diffusion weighted image denoising using overcomplete local PCA. *PloS one* **8** (2013).
- Tabesh, A., Jensen, J. H., Ardekani, B. A. & Helpert, J. A. Estimation of tensors and tensor-derived measures in diffusional kurtosis imaging. *Magn Reson Med* **65**, 823–836. <https://doi.org/10.1002/mrm.22655> (2011).
- Schmidt, P. *et al.* An automated tool for detection of FLAIR-hyperintense white-matter lesions in multiple sclerosis. *Neuroimage* **59**, 3774–3783 (2012).
- Najdenovska, E. *et al.* In-vivo probabilistic atlas of human thalamic nuclei based on diffusion-weighted magnetic resonance imaging. *Sci. Data* **5**, 180270 (2018).

Acknowledgements

The authors thank the patients and their caregivers for their time and commitment to this research. The first author also thanks Dr. Chung-Ping Lo and Dr. Ching-Feng Huang for their continued support of research work.

Author contributions

MCT and LWK: study concept and design, analysis, interpretation, and drafting of the manuscript. SMH: image processing and analysis. YHH: neuropsychological test assessment. JJY and CYL: neuroimaging data collection. All authors contributed to writing the manuscript.

Funding

This work was supported by research grants from Taichung Tzu Chi Hospital (TTCRD 111-03 and TTCRD 112-04 for MCT), National Health Research Institutes (NHRI-111-BN-PP-06 for LWK), and the Ministry of Science

and Technology in Taiwan (NSTC-111-2221-E-400-001-MY2 for LWK and NSTC 111-2811-E-400-002-MY2 for SMH).

Competing interests

The authors have no relevant financial or non-financial interests to disclose.

Additional information

Supplementary Information The online version contains supplementary material available at <https://doi.org/10.1038/s41598-024-52910-x>.

Correspondence and requests for materials should be addressed to L.-W.K.

Reprints and permissions information is available at www.nature.com/reprints.

Publisher's note Springer Nature remains neutral with regard to jurisdictional claims in published maps and institutional affiliations.



Open Access This article is licensed under a Creative Commons Attribution 4.0 International License, which permits use, sharing, adaptation, distribution and reproduction in any medium or format, as long as you give appropriate credit to the original author(s) and the source, provide a link to the Creative Commons licence, and indicate if changes were made. The images or other third party material in this article are included in the article's Creative Commons licence, unless indicated otherwise in a credit line to the material. If material is not included in the article's Creative Commons licence and your intended use is not permitted by statutory regulation or exceeds the permitted use, you will need to obtain permission directly from the copyright holder. To view a copy of this licence, visit <http://creativecommons.org/licenses/by/4.0/>.

© The Author(s) 2024